

# Measurements of aircraft wake vortex parameters with a coherent Doppler lidar

I.N. Smalikho<sup>1</sup> and S. Rahm<sup>2</sup>

<sup>1</sup>*V.E. Zuev Institute of Atmospheric Optics,  
Siberian Branch of the Russian Academy of Sciences, Tomsk, Russia*

<sup>2</sup>*Institute of Atmospheric Physics,  
German Aerospace Center, Munich, Germany*

Received April 11, 2008

Methods and results of coherent Doppler lidar measurements of aircraft wake vortex parameters are reviewed. The results were obtained from data measured by a pulsed 2- $\mu$ m lidar and continuous-wave CO<sub>2</sub> lidars in 2001–2007.

## Introduction

Vortices generated by a flying aircraft can be dangerous for another aircraft following not far from the first one. In particular, this problem imposes certain limits on capacities of airports with the intensive use of runways. For air transport safety, it is necessary to know the minimal distance between aircrafts following one after another especially in the case of vortex generation by a big aircraft. Such distance depends on the aircraft wake vortex intensity (aircraft type); the vortex lifetime is essentially determined by dynamic state of the atmosphere (turbulence and vertical wind gradient). In this connection, the study of aircraft wake vortex evolution at different state of the atmosphere and aircraft type is of current interest.

Coherent Doppler lidars can be used both for measurements of wind and atmospheric dynamic turbulence<sup>1–13</sup> and the study of aircraft wake vortices.<sup>14–27</sup> There are two types of Doppler lidars: continuous-wave (cw) and pulsed. They are usable both in the ground configuration (a container with a lidar stands on the Earth's surface) and aircraft one (a lidar is mounted onboard some aircraft).

In 2001–2007, the Lidar Group from the Institute of Atmospheric Physics, German Aerospace center (DLR, Oberpfaffenhofen) measured aircraft wake vortices by two own Doppler lidars, i.e., cw CO<sub>2</sub> lidar (2001 and 2003) and pulsed 2- $\mu$ m lidar (2002–2007). Two groups of specialists from France (ONERA, 2001–2003) and Great Britain (QinetiQ, 2001 and 2002) took part in the experiments with their own cw Doppler CO<sub>2</sub> lidars. Prior 2005, only ground measurements were carried out. About 1500 profiles of characteristics of couples of vortices (the coordinates of vortex center and its intensity, i.e., air velocity circulation about a closed path around the vortex axis, depending on time), generated by aircrafts of different types, have been restored from the data measured in this period (85% were obtained

by the pulsed 2- $\mu$ m lidar). Both ground and aircraft lidar measurement data were used. The measurement results and methods for experimental data processing have been published in Refs. 23–27.

First experiments were carried out by the above three groups in spring of 2001 near the Oberpfaffenhofen town. To measure parameters of vortices generated by a small aircraft (ATTAS [Ref. 23]), three cw Doppler CO<sub>2</sub> lidars were used. The necessity of the use of at least two cw lidars, spaced by some distance, is caused by impossibility of determining the distance to the aircraft wake vortex axis with an acceptable accuracy from the data of one such lidar.<sup>23</sup> This problem is absent when using one pulsed Doppler lidar. Besides, in contrast to two scanning cw lidars, a pulsed lidar with optimally chosen sensing-beam scanning allows a longer observation of vortex evolution, especially from large aircrafts generating long-living vortices.

In the following experiments, carried out in France at the airport of the Tarbes town in summer of 2002, the research group from DLR used a pulsed 2- $\mu$ m Doppler lidar along with two cw lidars of ONERA and QinetiQ. An object of the study was vortices generated in the wake of a big transport aircraft (BTA). Independent simultaneous measurements by the pulsed lidar on the one hand and two cw lidars on the other hand allowed the accuracy of estimation of aircraft wake parameters to be found.<sup>25</sup> Next year, similar experiments were carried out at the same place with the use of the cw CO<sub>2</sub> lidar of DLR instead of the QinetiQ's lidar; to improve the signal-to-noise ratio, smoke generators were mounted on the wings of an aircraft used in the experiments.

From 2004 to 2007, aircraft wake vortices were studied by the Lidar Group from DLR with the use of only one pulsed 2- $\mu$ m lidar Doppler lidar. To study the influence of Earth's surface on the behavior of aircraft wake vortices, lidar measurements of vortices, generated by landing aircrafts, were carried

out at two strips of the Frankfurt am Main airport in 2004 (September–December). The ground lidar sensing of aircraft wake vortices out for different types of BTA and in different configurations was carried in France (Toulouse, May–June, 2005; Istres, July–December, 2005; Tarbes, April, 2007) and Germany (Oberpfaffenhofen, March and July–August, 2006).

Lidar measurements of aircraft wake vortices in the free atmosphere are possible only from onboard of another aircraft. Mounting the pulsed 2- $\mu\text{m}$  Doppler lidar in the DLR's research aircraft Falcon-20, we carried out the first measurements of vortices, generated by an ATTAS aircraft, in April, 2005. In 2006 (March, June, and November), similar experiments were carried out for the case of vortex generation by BTA of different types. The level of background aerosol is insufficient at high altitudes in the free atmosphere; therefore, for such lidar measurements, we mounted smoke generators on the wings of the aircraft, vortices from which were measured. Smoke generators were not used in March and June, 2006, because the weather conditions promoted condensation of moisture when emitting discharge gases from aircraft engine nozzles to the atmosphere.

During the period from 2001 to 2007, the experimental technique was modernized, the experience in lidar measurements was gained, and the algorithms for experimental data processing, developed by us, were repeatedly improved. This allowed vortex parameters estimates with higher accuracy and for greater numbers of situations realizable in the atmosphere.

In this work, the used techniques for coherent Doppler lidar measurements of aircraft wake vortex parameters are described as well as the methods for experimental data processing. The most characteristic measurement results are given.

## 1. Aircraft wake vortices

Formation of aerodynamic lift during aircraft moving is always accompanied by appearance of free vortices and their convergence into a flow. They turn into stable vertical bundles (Fig. 1) which can move after the aircraft for many kilometers.

The velocity for a couple of formed vortices can be presented as a superposition of fields of two isolated vortices<sup>28–30</sup>:

$$V^{(2)}(r) = V_1^{(1)}(r - r_1) + V_2^{(1)}(r - r_2), \quad (1)$$

where

$$V_i^{(1)}(r) = (-1)^i \frac{\Gamma_i \mu(|r|/r_C)}{2\pi r}$$

is the velocity of  $i$ th isolated vortex in the coordinates centered at the point  $r_i$  ( $r_i$  is the coordinates of the axis of the  $i$ th vortex,  $i = 1, 2$ );

$r = y + jz$  is the radius-vector;  $j = \sqrt{-1}$ ;  $z$  is the vertical coordinate;  $y$  is the horizontal coordinate in a plane normal to fly (Fig. 1);  $V = V_z + jV_y$ ,  $V_z$  and  $V_y$  are the vertical and horizontal components of the velocity;  $\Gamma_i$  is the circulation of the  $i$ th vortex;  $r_C$  is the vortex core radius. For the Lamb–Osin model,<sup>28,29</sup>

$$\mu(x) = 1 - \exp(-1.256x^2).$$

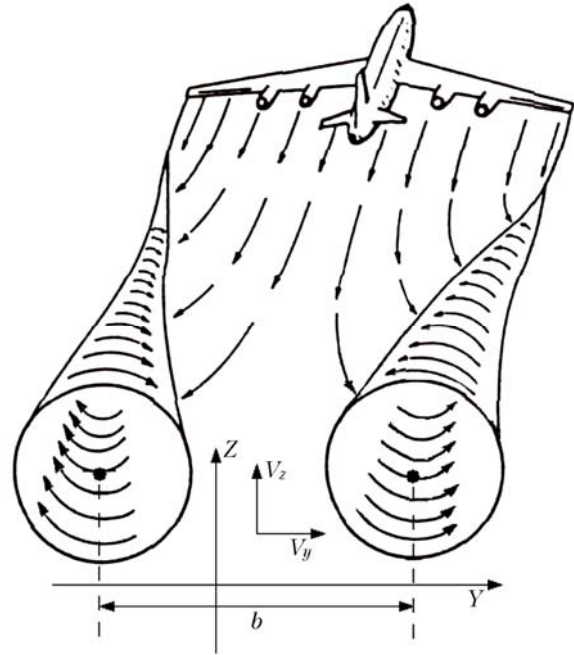


Fig. 1. Generation of vortices into the wake of a flying aircraft.

As aircraft wake vortices are in the field of each other, their cores move down with time (in the absence of strong upward wind). As it follows from Eq. (1), the lowering speed of vortices  $\omega$  in the unperturbed atmosphere at  $\Gamma_1 = \Gamma_2 = \Gamma$  is defined as  $\omega = \Gamma/(2\pi b)$ , where  $b = |r_1 - r_2|$  is the distance between vortices' centers. According to the theory (elliptic model),<sup>29</sup> the initial distance between vortices' centers is  $b_0 = (\pi/4)B_a$ , where  $B_a$  is the aircraft wing span. Correspondingly, the initial lowering speed of vortices is

$$\omega_0 = \Gamma_0/(2\pi b_0),$$

where  $\Gamma_0$  is the initial vortex circulation, which can be calculated by the equation<sup>29</sup>

$$\Gamma_0 = M_a g / (\rho b_0 V_a); \quad (2)$$

$g$  is the free fall acceleration;  $\rho$  is the air density at the flight altitude;  $M_a$  is the mass and  $V_a$  is the speed of aircraft. Knowing  $b_0$  and  $\Gamma_0$ , it is possible to calculate the time, at which the vortices move down

to the distance, equal to the distance between the vortices' centers ( $t_0 = b_0/w_0$ ), using the equation

$$t_0 = 2\pi b_0^2 / \Gamma_0. \quad (3)$$

The calculated  $b_0$ ,  $\Gamma_0$ , and  $t_0$  are often used to normalize the results of aircraft wake vortices measurements.

Dynamic processes in the atmosphere essentially influence the behavior of aircraft wake vortices. The vortices are transported by wind. Turbulent small-scale ( $\leq b_0$ ) wind inhomogeneities and vertical wind shifts can result in destruction of the vortices and their rapid decay. An aircraft flying at altitudes of several  $b_0$  is noticeably influenced by the Earth's surface. A two-phase wake vortex decay model was suggested in Refs. 31, 33: first a slow degradation of vortices circulation and then their rapid decay. The moment of transition from one to another decay phases depends on the turbulence intensity (rate of turbulence kinetic energy dissipation).

The invention of coherent Doppler lidars allowed the most complete experimental study of aircraft wake vortices.

## 2. Coherent Doppler lidars

The principle of operation of the coherent Doppler lidars (CDL) is based on sending the laser radiation to the atmosphere and coherent detection of the light scattered by aerosol particles. The speed of particles moving with an air current is determined from the measured frequency shift of the backscattered optical wave. Key elements of CDL are lasers generated the sensing and reference beams, telescope, and detectors. To change the angle of the sensing beam direction, a scanner is used. Below we briefly describe lidars, which were used for aircraft wake vortex sensing.

### 2.1. Cw lidars

Continuous-wave coherent Doppler CO<sub>2</sub> lidars, belonging to ONERA and QinetiQ, have similar specifications. In contrast to these two lidars (heterodyne systems), a cw CO<sub>2</sub> CDL, used by the Group from DLR, is a homodyne system. These lidars are described in Refs. 16 and 21 in detail. The lidars are monostatic with a transmitting-receiving telescope. The telescope aperture is of 30 cm in diameter. Focusing of the sensing beam allows the formation of sensed volume with the longitudinal size  $\delta R \sim R^2$  [Ref. 34], where the focus length  $R$  determines the measurement range. The longitudinal size of the sensed volume  $\delta R \approx 10$  m at  $R = 100$  m, while  $\delta R \approx 88$  m at  $R = 300$  m, which is similar to the case of pulsed CDL.<sup>25</sup> During lidar operation, signal spectra are recorded every 50  $\mu$ s by a spectral analyzer and then averaged. The frequency resolution in the obtained spectra answers the 0.1 m/s-speed resolution.

### 2.2. Pulsed lidar

The pulsed 2- $\mu$ m CDL was designed on the basis of a MAG-1 transmitting-receiving device using Photonics CLR.<sup>35</sup> It includes two 2.022- $\mu$ m Tm:LuAG lasers pumped by light emitting diodes. The master laser generates a continuous-wave beam, which splits into two beams, one of which is injected into the pulsed laser and another one, passing through a photoacoustic modulator (frequency shift  $\delta f \sim 100$  MHz), is used as a reference beam. The generated pulse is 2 mJ in power and 400 ns in width. The pulse shape (radiation power versus time) is close to Gaussian. The pulse radiation beam splits into sensing and control ones. Sensing pulses (a repetition rate of 500 Hz) are sent to the atmosphere through the transmitting-receiving telescope (an aperture diameter of 180 mm). The radiation, scattered in the atmosphere, is focused by the telescope, mixed with the reference beam, and then is sent to the photodetector active area. To control the intermediate frequency  $\delta f$ , the control pulse beam is also mixed with the reference one and is detected with another photodetector. The detected signals (backscattered and control) are digitized with a frequency of 500 MHz.

## 3. Measurement strategy

To find parameters of aircraft wake vortex, it is necessary to know the spatial distribution of its tangential speed. CDL, being at some distance from the aircraft wake, allows one to obtain such distribution by means of scanning by the sensing beam in a plane normal to the direction of the aircraft movement. An acceptable spatiotemporal distribution of a lidar-measured parameter is realizable at optimal choice of the measurement geometry and angular scanning velocity.

### 3.1. Ground measurements

Figure 2 shows the geometry of lidar measurements of aircraft wake vortices at the airfield in Tarbes (July, 2002).

The distance between ONERA (L3) and QinetiQ (L2) cw CDLs was 122 m. The pulsed CDL (L1) was placed at 824 m from L3 at a small angle to the Y-axis (Fig. 2, top view). While measuring the vortices, generated by a BTA, sensing beams were scanned within the limits shown in Fig. 2 (side view) with rates of 2 (L1), 10 (L2), and 12 deg/s (L3). The aircraft circled in the measurement site, flying along a line parallel to the X-axis, with a period of {Z, Y}-plane intersection of about 8 min. The flight altitude varied within 180–430 m. Geometries of cw CDL measurements in Oberpfaffenhofen (2001) and Tarbes (2003) were similar. The data measured by L2 and L3 allow only estimates of parameters of aircraft wake vortices within the area of scanning sectors intersection (see Fig. 2).

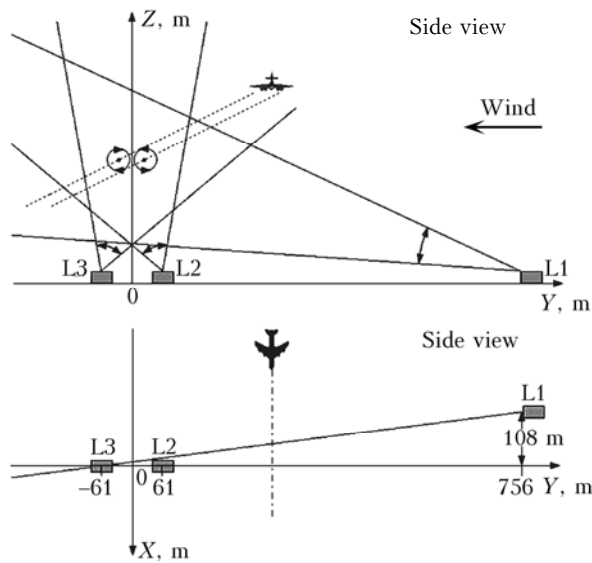


**Fig. 2.** Geometry of lidar measurements at the airfield in Tarbes: L1 is the pulsed CDL; L2 and L3 are the cw CDLs. Dashed lines show the trajectories of cores of aircraft wake vortices, transported by wind.

At strong side wind, such measurements could not be long. The use of a pulsed lidar (L1) usually allows development of aircraft wake vortices till their total decay. Since 2004, we have used only the pulsed CDL with the measurement geometry similar to those shown in Fig. 2 for this lidar.

### 3.2. Aircraft measurements

Ground Doppler lidar measurements of aircraft wake vortices are possible only in the boundary air layer. When an aircraft flies in the free atmosphere, the generated vortices can be measured only with a CDL, mounted onboard the another aircraft. Such measurements were realized by the DLR Lidar Group in Bavaria in 2005 and in the South France in 2006. A pulsed 2- $\mu\text{m}$  CDL was mounted onboard the Falcon-20 aircraft. Other used aircrafts (vortices of which were measured) were ATTAS in 2005 and BTA in 2006.

Figure 3 shows the basic aircraft lidar measurement schematic used in these experiments. During the lidar measurements, Falcon-20 (A1) circled at a fixed altitude. The altitude in different experiments was from 3 to 12 km.

Another aircraft (ATTAS, BTA) designated in Fig. 3 as A2, circled in opposite direction at a lower altitude. As a rule, the difference in A1 and A2 flight altitudes was 900 m. The sensing beam was scanned with a rate of 10 deg/s. Maximal and minimal scanning angles (relative to the vertical axis) were +15 and  $-15^\circ$ , respectively. Smoke generators were mounted on the wings of A2 aircraft. They allowed the power of scattered lidar signal to be sufficient to measure aircraft wake vortices of different ages.

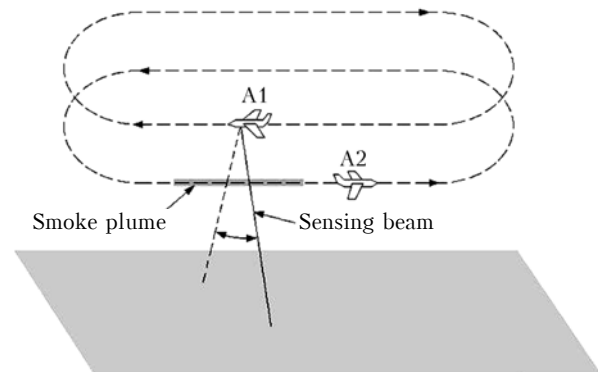


**Fig. 3.** Basic schematic of CDL measurement of vortices, generated by A2 aircraft (ATTAS or BTA), from onboard the A1 aircraft (Falcon-20).

Besides, a Falcon pilot could see the smoke plume and correct the flight trajectory for the smoke plume to be always within the sensing-beam scanning sector. These experiments are described in Refs. 26 and 27 in more detail. In March and June, 2006, smoke generators were not used, since the aircraft wake was visible due to condensation of moisture (A1 flight altitude was about 11–12 km).

## 4. Experimental data processing

After the finish of the experiment, initial data of lidar measurements were processed to obtain aircraft wake vortex parameters. Such estimates are possible from the data of two cw or one pulsed CDL.

### 4.1. Estimation of vortex parameters from cw lidar measurements

An example of Doppler spectra, measured by the DLR Lidar Group with the use of a cw CDL, is shown in Fig. 4a.

The values of spectra  $S_D$  at every point  $(V, t)$  are shown in relative units with the help of the black-and-white color scale, where  $t$  is the time (abscissa) passed after appearance of aircraft wake vortices (after intersection of the sensing-beam scanning plane by the aircraft). With accounting for the Doppler relation

$$V = f\lambda/2,$$

where  $f$  is the frequency and  $\lambda$  is the optical wavelength, spectra are presented as a function of velocity  $V$  (ordinate axis). Here 375 spectra  $S_D(V)$  are shown, measured every 13.3 ms when scanning by the sensing-beam. The dashed-dotted line in Fig. 4b corresponds to the scanning angle  $\varphi$  for the considered time period.

The Doppler spectrum  $S_D(V)$  is a weighted velocity distribution (velocities projections to the beam axis) of scattering particles in a sensed volume. If the focal length  $R$  is close (as in our example) to the distance between the lidar and aircraft wake

vortex core, then the transverse profile of the later is well seen in the measured spectra (see Fig. 4a).

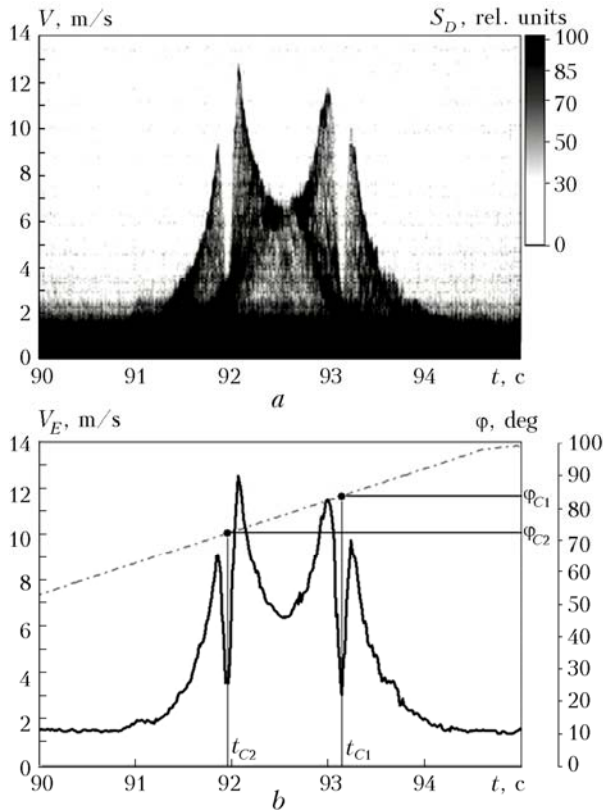


**Fig. 4.** Doppler spectra (a) and velocity envelope (b), measured by the DLR's cw lidar in the vicinity of a couple of aircraft wake vortices.

The velocity envelope  $V_E[\varphi(t)]$ , corresponding to the distribution of tangential speed around the vortex core, can be obtained from the spectra by means of setting a certain threshold spectrum value  $Thr$  and finding  $V_E$  via intersection of the spectral curve  $S_D(V)$  with  $Thr$  (i.e.,  $S_D(V_E) = Thr$ ). The velocity envelope  $V_E[\varphi(t)]$  is shown in Fig. 4b by the solid curve. The intersection angles of the sensing beam with the axes of right ( $\varphi_{C1}$ ) and left ( $\varphi_{C2}$ ) vortices can be determined from  $V_E[\varphi(t)]$ . At the known distance between the lidar and the core of  $i$ th vortex ( $i = 1$  for the right and  $i = 2$  for the left vortices), the vortex circulation  $\hat{\Gamma}_i$  can be estimated by integration<sup>36</sup>:

$$\hat{\Gamma}_i = \frac{1}{N} \sum_n^N 2\pi |V_E(\varphi_n)| r_i(\varphi_n), \quad (4)$$

where

$$r_i(\varphi_n) = R_{Ci} |\sin(\varphi_n - \varphi_{Ci})|$$

is the distance corresponding to the radius of a circle with the center coinciding with the axis of the  $i$ th vortex. The summation in Eq. (4) is carried out over values of  $n$ , satisfying the condition

$$r_{\min} \leq r_i(\varphi_n) \leq r_{\max}.$$

Integration intervals  $[r_{\min}, r_{\max}]$  were set as follows:  $r_{\min} = 3$  m and  $r_{\max} = 8$  m in case of small aircrafts (e.g., ATTAS) and  $r_{\min} = 5$  m and  $r_{\max} = 15$  m in case of BTA.

When measuring by one cw CDL, the distance  $R_{Ci}$  is unknown, and change of  $R_{Ci}$  to  $R$  in Eq. (4) can give a large error. Therefore, another one lidar is required for measurements of aircraft wake vortex parameters. Since the ONERA and QinetiQ cw lidars are heterodyne systems (intermediate frequency  $\delta f \neq 0$ ), the speed and direction (along the sensing beam axis) of movement of scattering particles can be determined from spectra, measured by these lidars. Examples of such spectra are given in Refs. 21, 23, and 36.

In contrast to the DLR's cw lidar (where  $\delta f = 0$ ), here it is necessary to obtain two velocity envelopes – positive and negative – from the measured spectra. Again, after finding the angles  $\varphi_{C1}$  and  $\varphi_{C2}$  and the corresponding combination of the positive and negative velocity envelopes, we obtain  $V_E[\varphi(t)] \equiv V_E(\varphi_n)$ , used in Eq. (4). The coordinates of aircraft wake vortex core are estimated from the data of L2 and L3 lidars (see Fig. 2) by means of triangulation

The coordinates of vortex center  $\{z_{Ci}(t), y_{Ci}(t)\}$  and the distance from L2 (L3) to the axes of the  $i$ th vortex, respectively, are estimated from the obtained intersection angles of vortex axis with sensing beam  $\varphi_{Ci}^{L2}(t_{Ci})$  (L2 data) and  $\varphi_{Ci}^{L3}(t'_{Ci})$  (L3 data) (usually  $t_{Ci} \neq t'_{Ci}$ ) by the smoothing Kalman filter.<sup>23,37</sup> Then the circulation is calculated by Eq. (4).

#### 4.2. Estimation of vortex parameters from measurements by the pulsed lidar

Processing of data measured by the pulsed 2- $\mu$ m CDL with the purpose of obtaining information of aircraft wake vortices, includes three main steps: estimation of Doppler spectra, coordinates of vortex core, and vortex circulation.

##### Doppler spectra

An example of initial lidar data, measured at the  $i$ th sending a pulse to the atmosphere ( $i = 1, 2, 3, \dots$ ) is shown in Fig. 5, including the control and backscattering signals. The intermediate frequency  $\delta f^{(i)}$  (corresponding to zero velocity) is determined from the control signal, the pulsing time  $t_0^{(i)} = m_0^{(i)} T_s$ , where  $T_s = 2$  ns is the recording time of one signal, and the pulsewidth is  $\sigma_p$ . The backscattering signal  $J_B(mT_s, \varphi_i)$ , measured at the scanning angle  $\varphi_i$ , can be considered as a function of time  $t_R = mT_s - t_0^{(i)}$  after pulse emission in the atmosphere or of distance  $R = ct_R/2$  ( $c$  is the light speed) from the lidar to the center of the sensed volume.

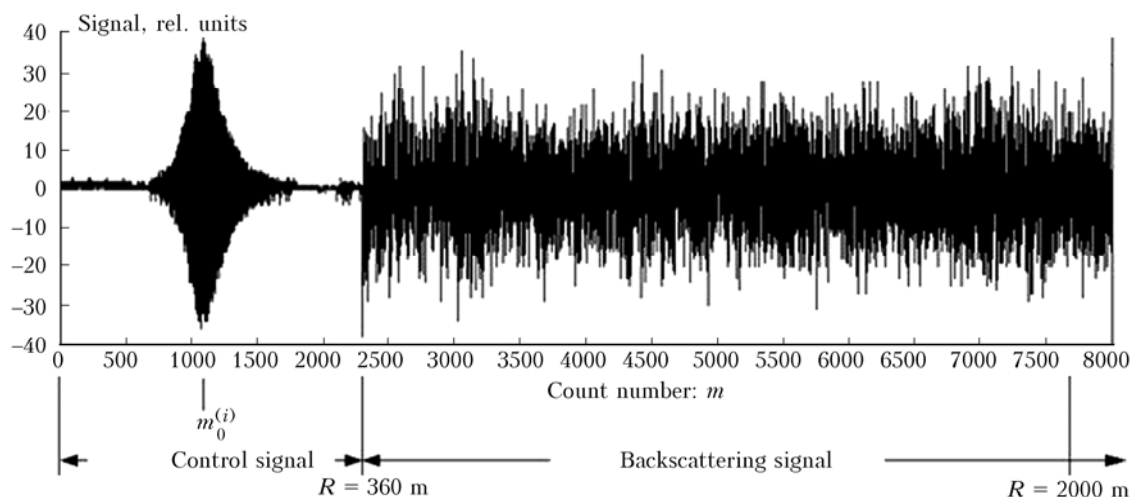


Fig. 5. Characteristic example of initial data of the 2- $\mu$ m CDL measured at sending a single sensing pulse to the atmosphere.

To obtain Doppler spectra at different sensing ranges  $R_l$ , we choose  $M$  signal counts  $J_B(mT_s, \varphi_i)$  around the corresponding count number  $m$  and multiply this array by the of Gaussian window function

$$W(mT_s) = \left( \frac{T_s}{\sqrt{\pi}\sigma_W} \right)^{1/2} \exp \left[ -\frac{(m - M/2)^2 T_s^2}{2\sigma_W^2} \right],$$

i.e., we have

$$\begin{aligned} J_W(mT_s, R_l, \varphi_i) &= \\ &= J_B \left( ([R_l / (cT_s / 2)] + m_0^{(i)} - M/2 + m)T_s, \varphi_i \right) W(mT_s), \end{aligned} \quad (5)$$

where  $R_l = R_0 + \Delta Rl$ ;  $l=0, 1, 2, \dots, L$ ;  $M = 2048$ . To estimate aircraft wake vortex parameters from the lidar data, an optimal step is  $\Delta R = 12$  m. In the majority of cases, we set the minimal distance  $R_0$  equal to 500 m, and  $L$  did not exceed 100. The width of Gaussian window  $\sigma_W$  was set equal to the pulsewidth  $\sigma_p$ . In this case, the longitudinal spatial distribution (longitudinal size of the sensed volume) was about 94 m. Using FFT, estimate the power spectra of backscattering signal (Doppler spectra):

$$\hat{S}_D(\Delta f k, R_l, \varphi_i) = \left| \sum_{m'=0}^{M-1} J_W(m'T_s, R_l, \varphi_i) \exp(-2\pi j k m' / M) \right|^2, \quad (6)$$

where  $k=0, 1, 2, \dots, M-1$ ;  $\Delta f = (MT_s)^{-1} = 0.244$  MHz.

The level of fluctuations of the spectral estimates can be decreased by means of their averaging, i.e., using the equation

$$S_D(f_k, R_l, \varphi_n) = N_a^{-1} \sum_{i=1}^{N_a} \hat{S}_D(\Delta f k - \delta f^{(i)}, R_l, \varphi_i). \quad (7)$$

The intermediate frequency  $\delta f^{(i)}$ ,  $i=(n-1)N_a + i'$ ;  $n=1, 2, 3, \dots$  is also taken into account in Eq. (7). For averaging, we set  $N_a=25$  in the ground measurements and  $N_a=5$  in the aircraft ones. Considering the pulse frequency rate equal to 500 Hz, and sensing-beam scanning velocity equal to 2 deg/s in the ground measurements and 10 deg/s in aircraft ones, the angular resolution was about 0.1 deg and, hence, the transversal spatial distribution was about 1.7 m at sensing range  $R=1$  km. Such a resolution is quite acceptable for estimation of vortex parameters. After normalizing the Doppler spectra to a mean noise spectrum component, we obtain a 3D array of normalized spectra  $S_D(f_k, R_l, \varphi_n)$ , where the frequency  $f_k$  can be changed to the velocity  $V_k = f_k \lambda / 2$  and the frequency (velocity) range can be narrowed to  $[-25$  m/s, 25 m/s].

An example of Doppler spectra, measured by the pulsed CDL (ground measurements, Frankfurt, 2004), is shown in Fig. 6.

The coordinates of cores of right and left vortices are shown in Fig. 6b. The spectrum, measured between these cores (the point of intersection of the horizontal and vertical lines), is shown in Fig. 6a. The spectra obtained at different ranges  $R$  and fixed angle  $\varphi$  are shown in Fig. 6c and at different  $\varphi$  and constant  $R$  in Fig. 6d.

#### Coordinates of the vortex core

Setting a certain threshold  $Thr$ , values for the positive  $V_{E+}$  and negative  $V_{E-}$  velocity envelopes can be obtained from the Doppler spectrum (see Fig. 6a). The  $Thr$  value is determined by the level of fluctuations of the noise spectrum component. This level depends on the number of averaging  $N_a$ . The probability of peak noise values excess over  $Thr$  is to be small. At the same time, the threshold  $Thr$  should not exceed very much the mean noise level:  $Thr=2.5$  and 3.5 at  $N_a=25$  and 5, respectively, are optimal values.

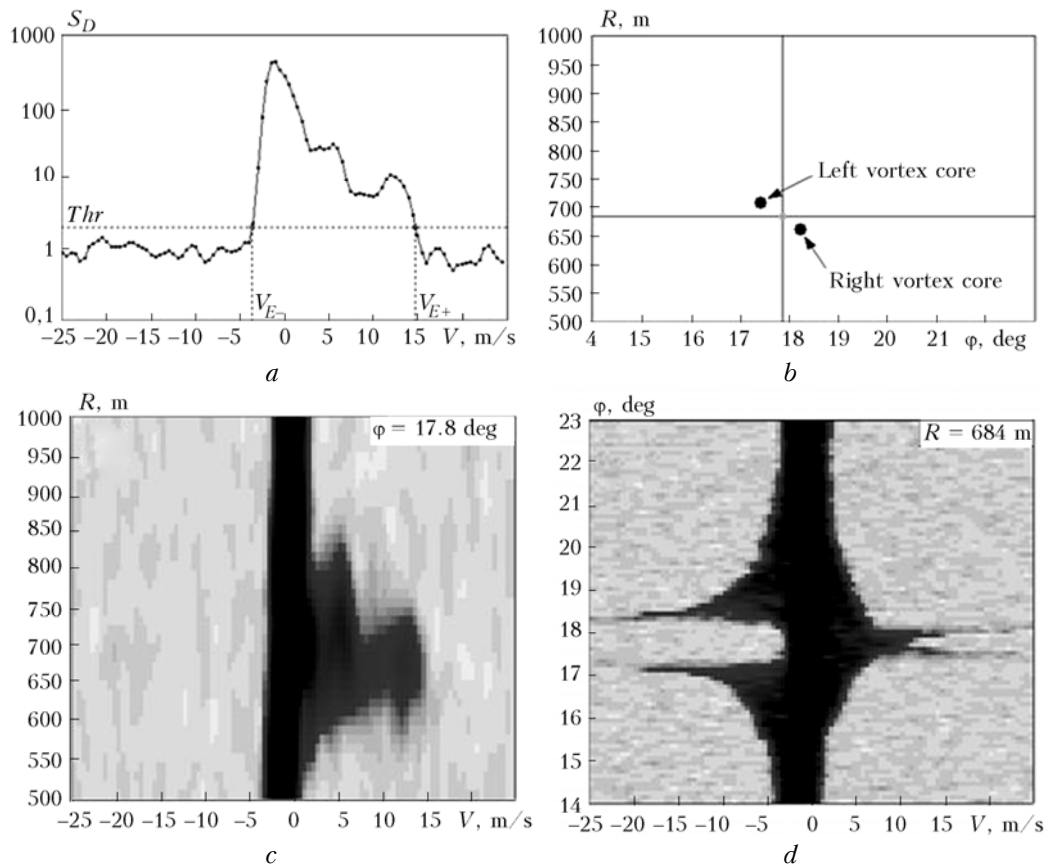


**Fig. 6.** Doppler spectra measured by the pulsed 2- $\mu\text{m}$  CDL: *a* – single spectrum at the point of vertical and horizontal image (*b*) lines intersection; *c* – spectra measured at different distances  $R$  from the lidar and the fixed scanning angle  $\varphi$ ; *d* – spectra measured at different  $\varphi$  and fixed  $R$ .

To determine the coordinates of aircraft wake vortex core, it is sufficient to use the  $Thr$  value common to any  $R_l$  and  $\varphi_n$ . The velocity envelopes  $V_{E+}(R_l, \varphi_n)$  and  $V_{E-}(R_l, \varphi_n)$  (measurements in Tarbes in 2003) are shown in Fig. 7, where the region with a couple of vortices is seen.

The coordinates  $\{R_{C1}, \varphi_{C1}\}$  and  $\{R_{C2}, \varphi_{C2}\}$  of the right and left vortices' cores are estimated separately as the equally-spaced positions between maximum of the positive velocity envelope and minimum of the negative one. The core position of the left vortex is

marked by the light circle and of the right vortex – by the grey one.

### Vortex circulation

The vortex core coordinates  $\{R_{C1}, \varphi_{C1}\}$ ,  $\{R_{C2}, \varphi_{C2}\}$  and the spectra

$$S_D(f_k - 2V_B / \lambda, R_{C1}, \varphi_n), S_D(f_k - 2V_B / \lambda, R_{C2}, \varphi_n),$$

where  $V_B$  is the radial velocity of the background wind, determined from the lidar measurement data,<sup>24</sup> can be used for estimating vortex circulation.

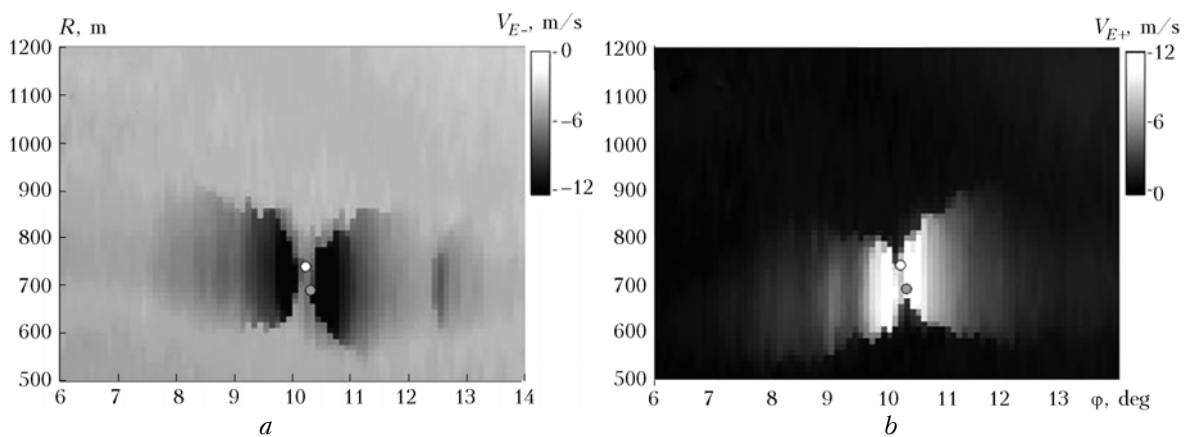


**Fig. 7.** Negative (*a*) and positive (*b*) velocity envelopes.

Figures 8a and b show the examples of such spectra (ground measurements, Frankfurt, 2004). Using  $Thr = 2.5$ , common for any angles  $\varphi_n$ , the positive  $V_{E+}(R_{Ci}, \varphi_n)$  and negative  $V_{E-}(R_{Ci}, \varphi_n)$  ( $i = 1, 2$ ) velocity envelopes (dashed lines in Figs. 8c and d) can be obtained from the Doppler spectra (Figs. 8a and b). Estimates of vortex circulation, obtained by integration (Eq. (4)), when using these velocity envelopes in grey regions in Figs. 8c and d ( $r_{\min} = 5$  m,  $r_{\max} = 15$  m), have a large error. As numerical experiments with the use of well-known algorithms for Doppler lidar signal modeling have shown,<sup>8,38-41</sup> an appropriate estimate of vortex circulation in such measurements is possible only by presetting the corresponding threshold  $Thr$  for every separate spectrum, i.e., the threshold  $Thr$  is to be a function of the scanning angle  $\varphi$ .

The so-called “floating” threshold  $Thr(\varphi)$  is calculated by a special algorithm, in which the theoretical spectrum model  $S_D^{(M)}(f, R, \varphi)$  is used, which is the average normalized Doppler spectrum. The formula for  $S_D^{(M)}(f, R, \varphi)$  was obtained in Ref. 42 for the case of homogeneous atmosphere and was generalized in Ref. 27 to the case of strong local inhomogeneity of the scattering medium properties,

caused by smoke or moisture condensation in an aircraft wake. This formula has the form

$$S_D^{(M)}(f, R, \varphi) = B \int_{-\infty}^{+\infty} dz' Q_S(z') \frac{S_a(R + z', \varphi) + S_b}{\sqrt{2\pi}\sigma_{fp}} \times \exp\left\{-\frac{[f - V_r(R + z', \varphi)2 / \lambda]^2}{2\sigma_{fp}^2}\right\} + 1, \quad (8)$$

where the frequency  $f \in [-B/2, B/2]$ ;  $B = 50$  MHz (50 m/s) is the transmission band;

$$Q_S(z') = \Delta z^{-1} \exp(-\pi z'^2 / \Delta z^2)$$

is the function of spatial resolution (averaging) along the axis of the sensing beam  $z'$ ;

$$\Delta z = \sqrt{\pi} \sqrt{\sigma_p^2 + \sigma_w^2} \cdot c / 2 \approx 94 \text{ m}$$

is the longitudinal size of the sensing volume;

$$\sigma_{fp} = \sqrt{\sigma_p^2 + \sigma_w^2} / (2\pi\sqrt{2}\sigma_p\sigma_w) \approx 0.65 \text{ MHz (0.65 m/s)}$$

is the instrumental widening of the spectrum. The sum  $S_a(R + z', \varphi) + S_b$  can be represented as a normalized density of the signal-to-noise ratio (SNR) distribution (the ratio of signal power to the noise

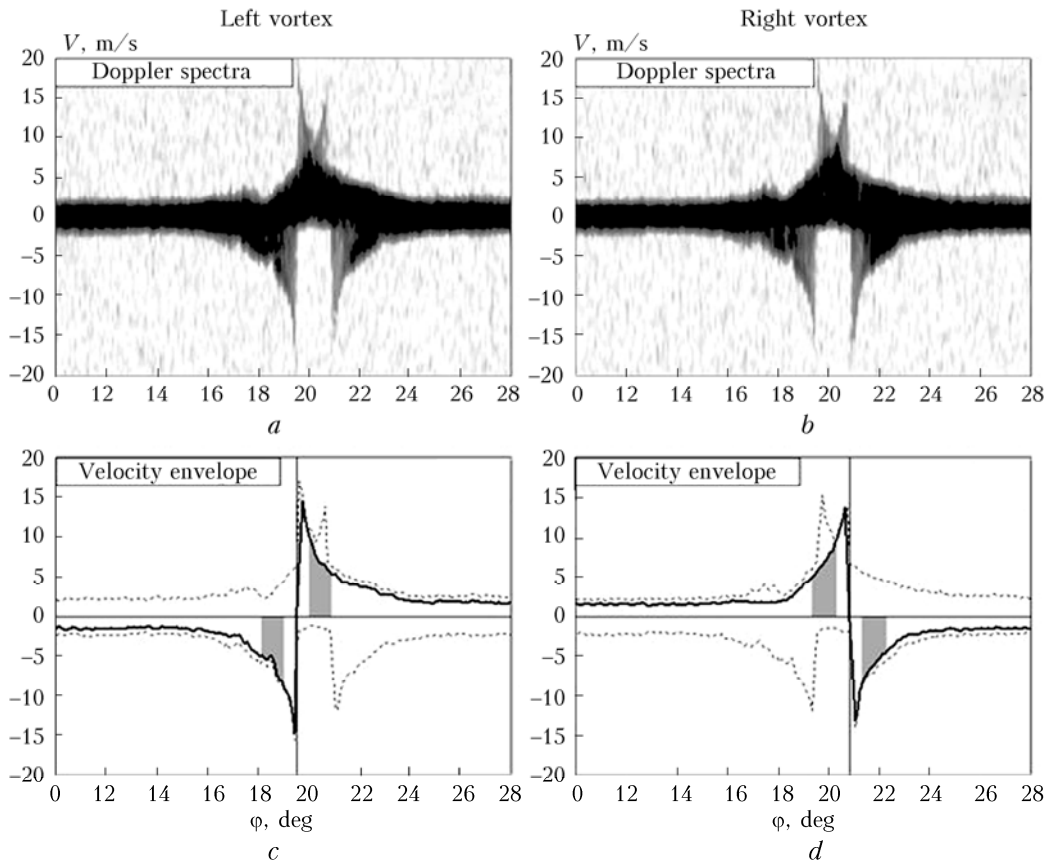


**Fig. 8.** Examples of Doppler spectra used for estimating circulation of the left (a) and right (b) aircraft wake vortices. The velocity envelopes [(c) and (d)] obtained from these spectra at fixed and “floating” thresholds are shown by dashed and solid curves, respectively.

power in the transmission band  $B=50$  MHz) along the axis  $z'$  with contributions of the generated smoke ( $[S_a(R+z',\varphi)]$ ) and the atmospheric aerosol ( $S_b$ ). In the absence of smoke,  $\text{SNR}=S_b$ . We used the Gaussian model<sup>27</sup> for  $S_a(R,\varphi)$ . Parameters of this model were determined from the measured Doppler spectra. The radial velocity  $V_r(R,\varphi)$  was calculated by the equation

$$V_r(R,\varphi) = \text{Im}[\Phi V^{(2)}(R\Phi)], \quad (9)$$

where  $\Phi = \cos\varphi + j\sin\varphi$  is the unit vector, directed along the beam axis, and the velocity  $V^{(2)}(R\Phi)$  is defined by Eq. (1).

If all parameters of the lidar and aircraft wake vortices (smoke plume) from Eqs. (8), (9), and (1) are known, then the thresholds for the right ( $i=1$ ) and left ( $i=2$ ) aircraft wake vortices can be found by the equation

$$\text{Thr}_i(\varphi) = S_D^{(M)}(f_{thr}^{(i)}(\varphi), R_{Ci}, \varphi), \quad (10)$$

where  $f_{thr}^{(i)}(\varphi) = V_r(R_{Ci}, \varphi)2/\lambda$  are calculated to the right and to the left of the vortex axis at the point  $\varphi = \varphi_{Ci}$ . If  $f_{thr}^{(i)}(\varphi) < 0$  and  $> 0$ , then  $V_{E-}(R_{Ci}, \varphi)$  and  $V_{E+}(R_{Ci}, \varphi)$  can be obtained from the measured spectra, respectively. Combining  $V_{E+}(R_{C1}, \varphi < \varphi_{C1})$  with  $V_{E-}(R_{C1}, \varphi > \varphi_{C1})$  for the right vortex and  $V_{E-}(R_{C2}, \varphi < \varphi_{C2})$  with  $V_{E+}(R_{C2}, \varphi > \varphi_{C2})$  for the left one, we obtain the velocity envelopes  $V_E(R_{C1}, \varphi)$  and  $V_E(R_{C2}, \varphi)$ , respectively, which can be used in Eq. (4) to calculate the circulation. But Eq. (1) includes the unknown circulation  $\Gamma_i$ . Therefore, to estimate the vortex circulation, an iterative procedure is used. As the first iteration, the estimates of  $\hat{\Gamma}_i$ , obtained from the velocity envelopes at  $\text{Thr} = \text{const}$  can be used (see dashed curves in Figs. 8c and d). Then the procedure is repeated with new  $V_{E-}(R_{Ci}, \varphi)$  and  $V_{E+}(R_{Ci}, \varphi)$ . This iterative procedure converges quite rapidly, as a rule, three iterations are enough. The resulted velocity envelopes  $V_E(R_{C1}, \varphi)$  and  $V_E(R_{C2}, \varphi)$  are shown by the solid curves in Figs. 8c and d.

## 5. Measurement results

Below, we present the results of ground lidar measurements in Tarbes in 2002 and in Frankfurt am Main in 2004, as well as the results of aircraft lidar measurements in the South France in November 2006. The measured parameters of vortices, generated by BTA, are analyzed.

### 5.1. Measurements in Tarbes

After successful experiments in Oberpfaffenhofen in 2001, where aircraft wake vortex parameters were measured by the cw Doppler lidar,<sup>23</sup> the next series of experiments took place in Tarbes in 2002, where capabilities of the pulsed CDL were tested. This study includes the comparative analysis of the results of simultaneous independent measurements of aircraft wake vortices by two cw and one pulsed lidar. In addition, data on the dissipation rate of turbulence

energy were derived from the pulsed CDL measurement results, which allowed analysis the lowering of aircraft wake vortices depending on the force of aircraft turbulence.

Measurements in Tarbes were carried out in June, 2002 (see P. 3.1 and Ref. 25). During four days, a BTA has crossed the measurement plane (ZY plane in Fig. 2) 65 times in total. One full scanning by the sensing beam of the pulsed lidar took 11 s. The beam crossed the axes of aircraft wake vortices with such periodicity on average, which is sufficient for detailed observation of the behavior (space movement) and development (lowering) of vortices. (See the brief description of techniques for data processing of the experiment in P. 4.)

Figure 9 shows the examples of pulsed lidar measured trajectories of aircraft wake vortex cores and the triangulation results obtained from measurements by two cw lidars.

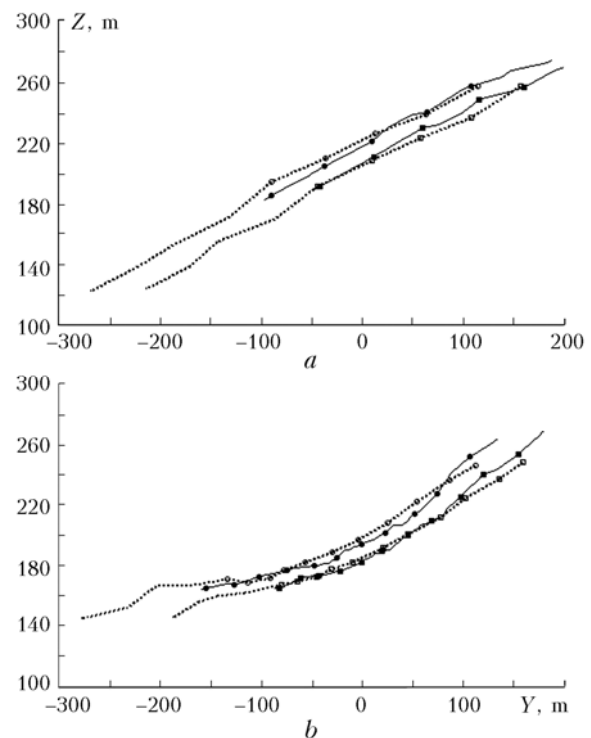


**Fig. 9.** Lidar-measured trajectories of aircraft wake vortex cores in Tarbes on June 13, 2002 at 21:34:03 (local time) (a) and June 14, 2002 at 20:13:11 (b): dashed curves correspond to the measurements by the pulsed CDL and solid ones – to the triangulation results obtained from measurements by two cw CDLs.

These measurements were carried out in June 13 and 14, 2002, at the X-transverse wind component equal to 4.5 (a) and 2.5 m/s (b). Aircraft coordinates (at  $X=0$ , see Fig. 2) for the examples in Fig. 9 were the following:  $Z=334$  m,  $Y=424$  m (a) and  $Z=347$  m,  $Y=297$  m (b). The vortex trajectories were measured by the pulsed CDL during 52–138 s (a) and 70–224 s (b) counted out after the aircraft passed the XY plane at  $X=0$ . The triangulation results were obtained for corresponding intervals 39–96 s (a) and 57–182 s (b).

It is seen from Fig. 9 that vortices go down with time and move to the left. The horizontal movement speeds are close to the above given speeds of the cross wind. The pulsed CDL observation time of aircraft wake vortices in these two examples was 78-s longer on average as compared to the cw lidar.

The moments of crossing vortex axes by the scanning beam differ for pulsed and cw lidars; therefore, linear interpolation was used to compare the results of simultaneous measurements. The following assessments of measurement precision were obtained<sup>25</sup> from the data shown in Fig. 10: 4.5 m for the vertical coordinate and 6.5 m for the horizontal one.

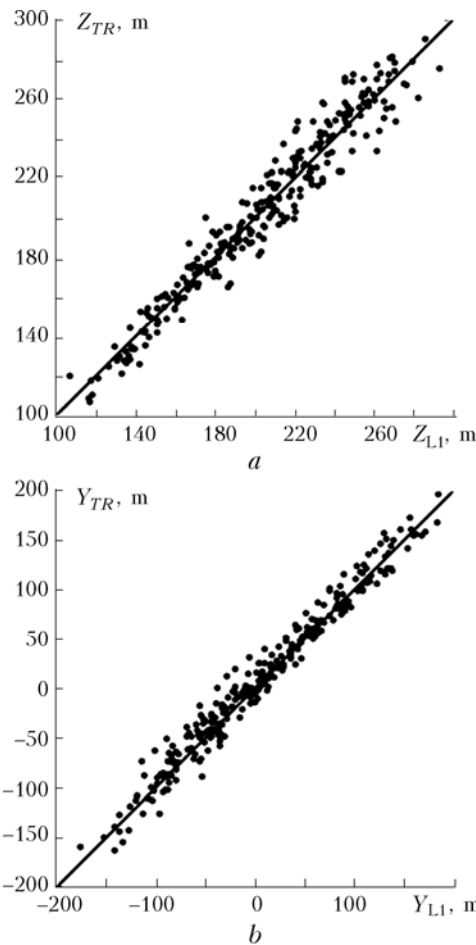


**Fig. 10.** Comparison of the triangulation results  $Z_{TR}$  and  $Y_{TR}$  with the pulsed-lidar measurements of the vertical  $Z_{L1}$  (a) and horizontal  $Y_{L1}$  (b) coordinates of aircraft wake vortex cores.

In contrast to the lidar L2, when measuring by the ONERA lidar (L3) the focus length  $R$  changed in accordance with the forecasting of the lowering of vortices and their transport by the cross wind. This allowed the sensing volume to be localized near the vortex core and, hence, obtaining of more precise data for velocity envelope, used in Eq. (4) to estimate the vortex circulation. For  $R_{Ci}$ , the results of triangulation were used, for which the measurement precision of angles  $\varphi_{Ci}$  by the cw lidars L2 and L3 was sufficient. Figure 11 shows three examples of

vortex circulation measurements with the use of the pulsed DLR (L1) and ONERA cw (L3) lidars. The dash lines show the theoretical values of initial circulation  $\Gamma_0$  calculated by Eq. (2). Vortex lowering with time  $t$  is shown. A good agreement between the data measured by the L1 and L2 lidars is evident.

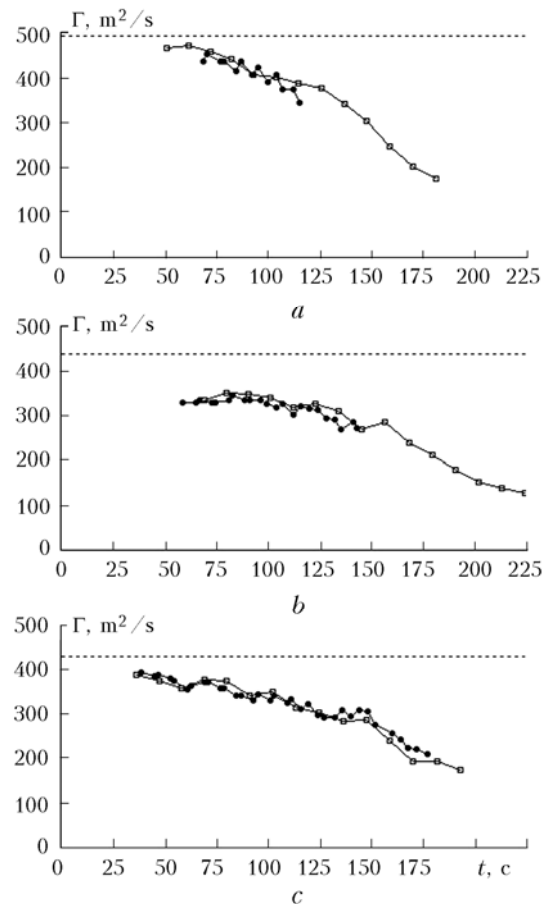


**Fig. 11.** Aircraft wake vortex circulation as a function of time, measured by the pulsed CDL (squares) and ONERA cw (circles) lidars in Tarbes in June 13, 2002 at 21:19:28 (local time) (a), June 14 at 20:13:11 (b), and June 17 at 20:31:14 (c).

Analysis of the results of aircraft wake vortex circulation with the pulsed DLR ( $\Gamma_{L1}$ ) and ONERA cw ( $\Gamma_{L3}$ ) lidars (Fig. 12 and Ref. 25) shows that the circulation measurement precision of these lidars is similar. Then, taking into account their independence and simultaneity, a measurement error of  $13 \text{ m}^2/\text{s}$  can be obtained from the data in Fig. 12.<sup>25</sup> Such precision is sufficient for studying the influence of wind turbulence on aircraft wake vortex decay.

The main reason of vortex decomposition in statistically homogeneous atmosphere is the small-scale turbulence described by the turbulence energy dissipation rate  $\varepsilon$ .<sup>43</sup> We derived the data on this parameter from the pulsed lidar L1 measurements.

The longitudinal structure velocity functions for different altitudes  $z$  were calculated from the measured radial wind speed, and then the altitude profile of dissipation rate  $\varepsilon(z)$  was retrieved. This

procedure is described in Ref. 13 in more detail. To avoid some overestimation of  $\varepsilon$  in this case, the data obtained in the regions of localization of aircraft wake vortices, were ignored. The profiles  $\varepsilon(z)$  for each measurement of circulation  $\Gamma(t)$  were averaged over the vortex observation altitudes. A range of averaged values  $5 \cdot 10^{-5} - 2 \cdot 10^{-3} \text{ m}^2/\text{s}^3$  was divided into three subranges:  $5 \cdot 10^{-5} - 2 \cdot 10^{-4}$ ,  $2 \cdot 10^{-4} - 5 \cdot 10^{-4}$ , and  $5 \cdot 10^{-4} - 2 \cdot 10^{-3} \text{ m}^2/\text{s}^3$ . The estimates of aircraft wake vortex circulation, obtained from the pulsed lidar data, were sorted within three corresponding groups.

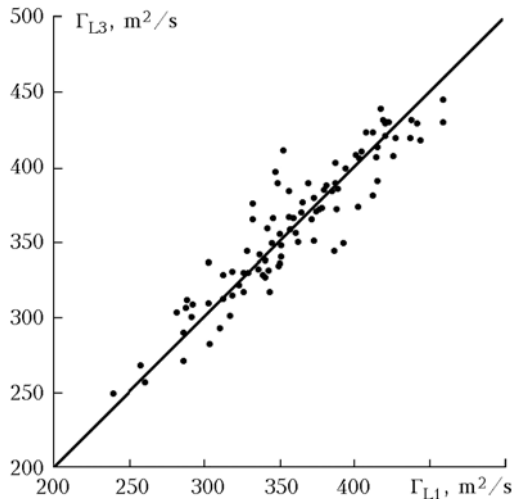


**Fig. 12.** Comparison of the results of simultaneous measurements of aircraft wake vortices circulation by the pulsed ( $\Gamma_{L1}$ ) and cw ( $\Gamma_{L3}$ ) CDLs.

Figure 13 shows the normalized aircraft wake vortex circulation  $\Gamma/\Gamma_0$  as a function of normalized time  $t/t_0$ , where  $t_0$  is calculated by Eq. (3).

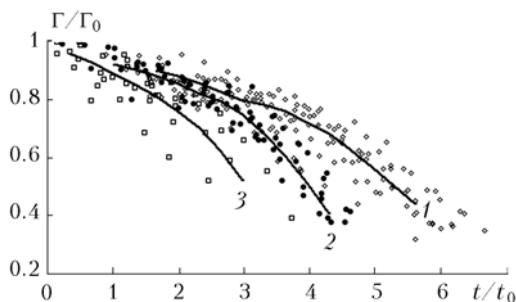


**Fig. 13.** Aircraft wake vortex circulation measured by the pulsed CDL at 1)  $\varepsilon \in [5 \cdot 10^{-5}, 2 \cdot 10^{-4}] \text{ m}^2/\text{s}^3$  (diamonds), 2)  $\varepsilon \in [2 \cdot 10^{-4}, 5 \cdot 10^{-4}] \text{ m}^2/\text{s}^3$  (circles), and 3)  $\varepsilon \in [5 \cdot 10^{-4}, 2 \cdot 10^{-3}] \text{ m}^2/\text{s}^3$  (squares). Curves 1, 2, and 3 show the average circulation as a function of time obtained for the given ranges of  $\varepsilon$ .

The signs show single circulation estimates and the curves show variation of the average circulation (smoothing averaging of single estimates) with time at different turbulence levels.

As is evident, the stronger turbulence, the more rapid decay of aircraft wake vortices. Two phases of the decay are observed: slow and rapid, that is in agreement with the theory developed in Refs. 31–33.

## 5.2. Measurements in Frankfurt am Main

To study the effect of the Earth's underlying surface on the behavior of aircraft wake vortices, the lidar group from DLR conducted two-stage measurements with the pulsed 2- $\mu\text{m}$  CDL at the Frankfurt am Main airport in 2004. First (September), the vortex parameters of aircraft flying at small altitudes of the boundary atmospheric layer, where the Earth's surface affects the vortices essentially, were measured during 9 days. Then (October–November) the measurements were carried out during 11 days at the altitudes, where the effect of Earth's surface on the behavior of aircraft wake vortices is negligible. Call such measurements the measurements under the Earth's surface effect (UESE) and beyond the Earth's surface effect (BESE).

In UESE measurements, the container with the lidar was located on the ground, in BESE – on the roof of a building of 20 m in height. Two runways of the airfield were used. The distances from the lidar to the runways were 500 and 1000 m. The lidar measured vortices, generated by landing scheduled aircrafts. The measurements usually began between 5:00 and 6:00 of local time, when the frequency of aircraft arrival rapidly increased and finished to the noon. Consider only the results of lidar measurements of aircraft wake vortex trajectories.

Figure 14 shows the trajectories of vortex cores measured without strong cross wind (*a* and *c*) and with it (*b* and *d*). In Fig. 14*a* (BESE measurements), only lowering of a couple of vortices is seen with virtually invariable distance between the vortices' cores. When aircraft wake vortices are generated at a small altitude, comparable with the wing span, without wind (Fig. 14*c*), the initial lowering of vortices changes to their ascent due to the surface repellency. In this case, the distance between the cores of right and left vortices increases. At strong cross wind, the Earth's surface the effect on the trajectories of aircraft wake vortices is not so evident (compare *b* and *d*).

The duration of the lidar continuous operation in these experiments was usually 5–6 h, when a quite large number of aircrafts of different types crossed the sensing-beam scanning plane. For example, in the period from 06:00 to 08:00, aircrafts landed on two runways with the 2-min interval on the average. The measurement results for one chosen type of BTA are given below. Such measured parameters as the altitude of vortex core  $Z$  and the distance between the cores of right and left vortices (see Fig. 14*c*) were normalized to the theoretical value of the initial distance between the vortices' cores  $b_0$ ; and the time  $t$ , counted from the beginning of generation of a couple of vortices, was normalized to the time  $t_0$  calculated by Eq. (3).

Figure 15 shows the time dependences of vortex core altitude and distance between the cores of the couple of vortices.

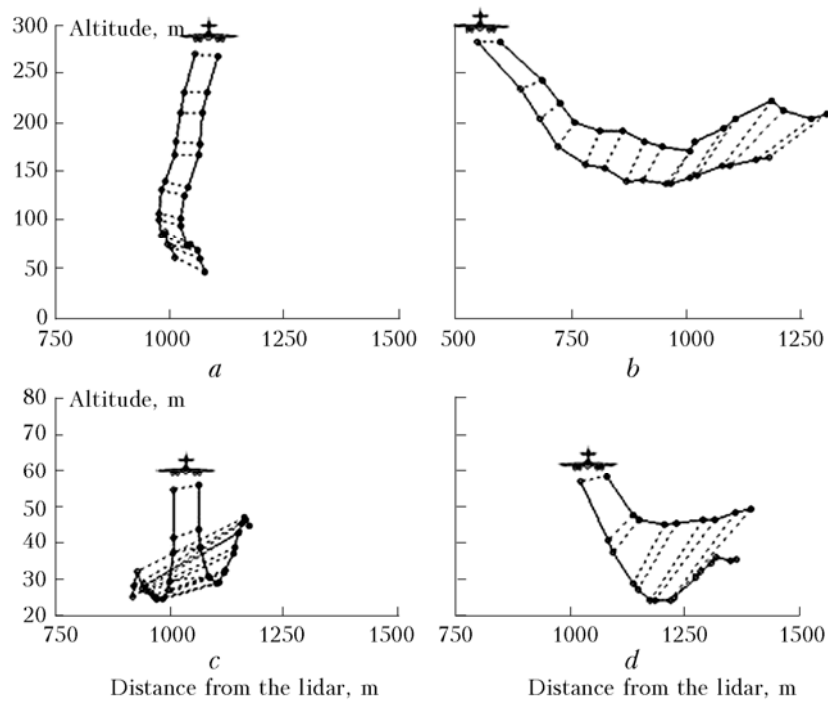


**Fig. 14.** Trajectories of aircraft wake vortices' cores CDL-measured in Frankfurt am Main in December 2 (*a*), October 19 (*b*), September 16 (*c*), and September 27 (*d*), 2004. The local times of the aircraft, crossing the measurement plane, were 09:38:44 (*a*), 05:05:46 (*b*), 08:21:31 (*c*), and 07:11:15 (*d*).

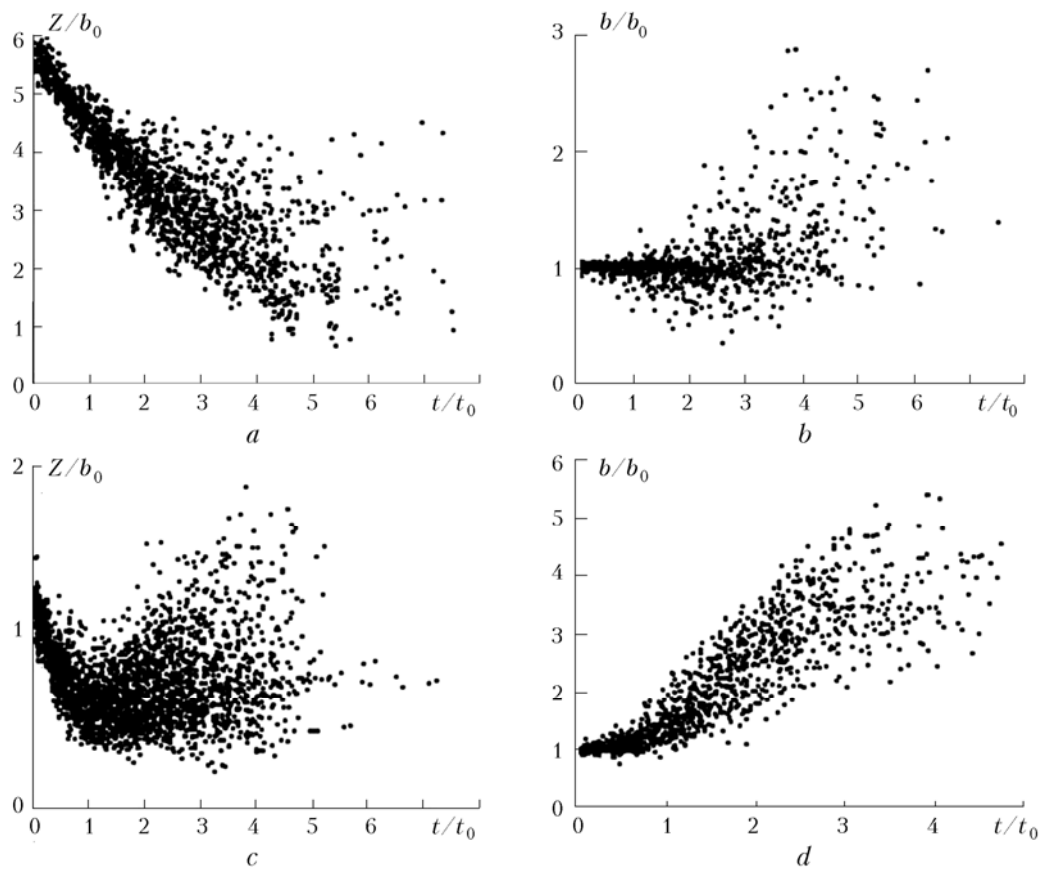


**Fig. 15.** Lidar-measured altitude of the core of an aircraft wake vortex [(*a*) and (*c*)] and distance between the cores of a couple of vortices [(*b*) and (*d*)]; (*a*), (*b*) are BESE and (*c*), (*d*) are UESE measurements.

As follows from analysis of the data in Fig. 15a, beyond the Earth's surface effect, the vortex lowering in the interval  $0 \leq t/t_0 \leq 3$  is on the average described by the linear time dependence:

$$\langle Z - Z_a \rangle / b_0 = -t/t_0,$$

where  $Z_a$  is the aircraft altitude in the measurement plane and  $\langle \dots \rangle$  is the sign of averaging. The further lowering is mainly connected with the decrease in vortex circulation. A similar linear dependence takes place for UESE measurements (Fig. 15c) at  $0 \leq t/t_0 < 1$ . Beyond this interval, vortices often reflect from the Earth's surface. In this case, the altitude of vortices ascend can exceed the altitude of BTA, generating them, and the vortices can be dangerous for a small landing aircraft.

The vortex, lowering to a certain critical altitude, rapidly decays due to strong friction against the Earth's surface. It is seen from Fig. 15d that the distance between the cores of the couple of vortices always increases with time under the Earth's surface effect. In contrast to this case, both increase and decrease in this distance can be observed in BESE measurements (Fig. 15b). The principal reason of an increase in the distance between the cores of a couple of vortices is wind shifts at the boundary of jet stream, often observable at a height of about 200–250 m in morning measurements. Vortices can rapidly decay at their close approach.

### 5.3. Aircraft measurements in November of 2006

Measurements of BTA-generated vortex parameters with the pulsed 2- $\mu$ m CDL, mounted onboard the Falcon-20 aircraft were carried out in November 9 (one flight, No. 1) and 15 (three flights, Nos. 2–4), 2006 between the Toulouse city and Pyrenees. The flight altitude was 2700 m (flights Nos. 1 and 2) and 3600 m (flights Nos. 3 and 4). The Falcon flew 900 m higher. The flight trajectories (GPS data) are shown in Ref. 27.

The rout of each flight included 8 sections, where smoke generators, mounted on BTA wings, switched on and lidar measurements were carried out from onboard the Falcon. At these sections, the Falcon and BTA flew in opposite directions (see Fig. 3), which allowed measurements at different distances from the BTA. The age of the measured vortex  $t$  was defined as  $t = R_a/V_a$ , where  $R_a$  was the distance from the vortex core position to the BTA;  $V_a$  was the real BTA airspeed. In contrast to the above-given results, we present the results here in a coordinate system centered at the BTA spatial position.

The estimates of normalized vertical coordinates of the aircraft wake vortex core  $Z/b_0$  are shown in Fig. 16 by dots, and the curve shows the mean value (the width of smoothing averaging window  $\delta t = t_0$ ) as a function of the normalized time  $t/t_0$ .

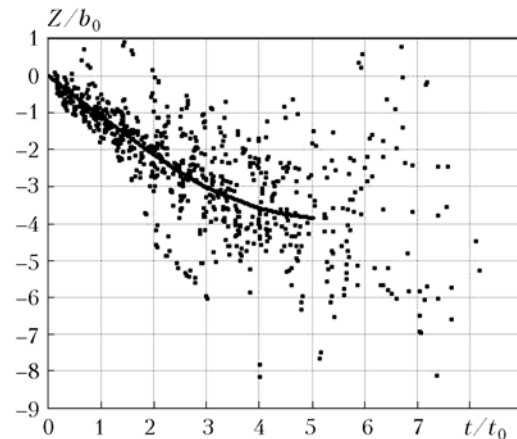


**Fig. 16.** Normalized vertical coordinates of aircraft wake vortex core in free atmosphere as a function of normalized time. The dots show single estimates from CDL measurement data, the curve shows mean values in a unit interval of the normalized time.

As is seen, the vortex lowering at  $t/t_0 < 3$  is on the average described by the linear time dependence  $\langle Z \rangle / b_0 = -t/t_0$ . Although the error of measurements of BTA and Falcon flight parameters (GPS data) contributes additionally to the estimation error of vortex core vertical coordinate, the reason of the wide spread of points in Fig. 16 is another.

Analysis of the lidar data, obtained in the first and second days, has shown the following. The wind was north in the first measurement day (November 9). The  $Z(t)$  dependences obtained from the data measured in this day are sufficiently smooth, and the spread in single estimates from the mean value correspond to the precision of vortex core vertical coordinate measurement, given in P. 5.1 (4.5 m). The wind was south in the second day, and air masses were transported by the wind over the Pyrenees to the measurement site. As a result, large-scale inhomogeneities with large values of the vertical component of wind speed  $|\tilde{V}_z|$  formed in the free atmosphere. The speed of aircraft wake vortex lowering at  $\tilde{V}_z < 0$  is larger and at  $\tilde{V}_z > 0$  smaller than the corresponding speed in unperturbed atmosphere. Data on the velocity  $\tilde{V}_z$  can be obtained from the lidar measurements. The background signal-to-noise ratio ( $S_b$ ) was sufficient to estimate  $\tilde{V}_z$ . Thus, in some measurements on March 15,  $|\tilde{V}_z|$  was larger than the initial speed of vortex lowering  $\omega_0 = b_0/t_0 \sim 1.5$  m/s, which explains both exceeding of zero level by some points in Fig. 16 and more significant lowering of vortices in comparison with the mean level (the curve in Fig. 16).

Despite such essential effect of mesoscale wind inhomogeneities  $\tilde{V}_z$ , they virtually do not affect the vortex circulation, since vortex decay in the considered case is mainly determined by the intensity of small-scale turbulence and the presence of wind shifts.

Figure 17 shows the aircraft-measured dependence of normalized vortex circulation  $\Gamma/\Gamma_0$  on the normalized time  $t/t_0$ .

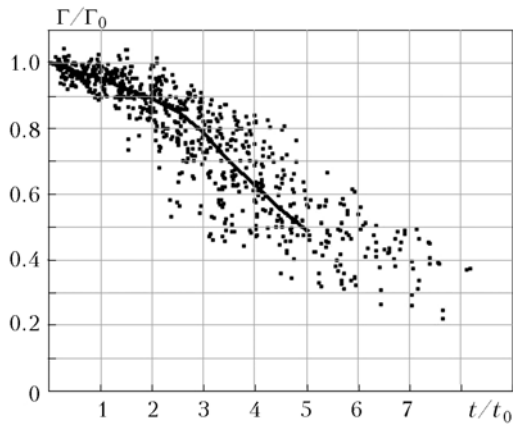


**Fig. 17.** Normalized aircraft wake vortex circulation in free atmosphere as a function of normalized time (the designations see in the capture to Fig. 16).

Dots show single estimates and the curve shows the mean circulation. As in case of measurements in the boundary atmospheric layer (see Fig. 13), this curve can be divided into two parts: 1) slow ( $0 < t/t_0 < 3$ ) and 2) rapid ( $t/t_0 > 3$ ) decay, which agrees with the theoretical model of two decay phases.<sup>31–33</sup> The moment of transition from one decay phase to another depends on the turbulence energy dissipation rate  $\varepsilon$ . It is impossible to estimate  $\varepsilon$  from the aircraft measurement data with an appropriate precision, because the signal-to-noise ratio beyond the smoke plume ( $\text{SNR} = S_b$ ) is too small.

## Conclusion

The performed experiments have shown the efficiency of coherent Doppler lidars in measurements of aircraft wake vortex parameters. The comparison of capabilities of cw and pulsed CDLs in such measurements shows that the pulsed lasers are preferable for measurements of aircraft wake vortices, which is especially important in aircraft measurements in free atmosphere. Second, in contrast to cw CDLs, a pulsed lidar allows one to trace the development of an aircraft wake vortex from its generation to complete decay.

The aircraft wake vortex circulation is the parameter, characterizing the level of hazard for another aircraft, appearing in the zone of localization of this vortex. An estimate of lidar circulation precision, obtained from the experimental data (see P. 5.1), allows CDL-study of aircraft wake vortices and, hence, the definition of safety zones for air transport, based on the study results for different weather conditions and flight patterns.

To find the conditions, when aircraft wake vortices can be measured by a Doppler lidar, we carried out numerical experiments consisted in lidar signal simulation<sup>8</sup> with the use of Lamb–Osin model

for a couple of vortices (Eq. (1)) and simulation data processing according to the scheme described in P. 4.2. Finally, it turned out that the error of circulation estimation from the simulation data on the average is the same as in experiments ( $13 \text{ m}^2/\text{s}$ ). If  $\text{SNR} < 1$ , the error sharply increases.

The maximum likelihood method, used in Ref. 41 for estimating aircraft wake vortex parameters, can well allow more accurate circulation estimates at  $\text{SNR} < 1$ . A disadvantage of the method in comparison with those described in this work, is large time expenses for computer processing of the lidar measurement data.

The condition  $\text{SNR} > 1$  was satisfied in zones of aircraft wake vortex localization in the majority of measurements with the pulsed  $2\text{-}\mu\text{m}$  CDL from 2002 to 2007 (especially in the use of smoke generators). Therefore, a large bulk of experimental data obtained in that period (core coordinates, aircraft wake vortex circulation, wind speed, parameters of atmospheric turbulence, aircraft data) is quite appropriate for further analysis aiming at solving the problems concerned with the safety of air transport.

## References

1. F. Köpp, R.L. Schwiesow, and Ch. Werner, *J. Climate Appl. Meteorol.* **23**, No. 1, 148–158 (1984).
2. F.F. Hall, R.M. Huffaker, R.M. Hardesty, M.E. Jackson, T.R. Lawrence, M.J. Post, R.A. Richter, and B.F. Weber, *Appl. Opt.* **23**, No. 15, 2503–2506 (1984).
3. J.G. Hawley, R. Tang, S.W. Henderson, C.P. Hale, M.J. Kavaya, and D. Moerder, *Appl. Opt.* **32**, No. 24, 4557–4568 (1993).
4. R. Frehlich, S.M. Hannon, and S.W. Henderson, *J. Atmos. and Ocean. Technol.* **11**, No. 6, 1517–1528 (1994).
5. Ch. Werner, P.H. Flamant, O. Reitebuch, F. Köpp, J. Streicher, S. Rahm, E. Nagel, M. Klier, H. Herrmann, C. Loth, P. Delville, Ph. Drobinski, B. Romand, Ch. Boitel, D. Oh, M. Lopez, M. Meissonner, D. Bruneau, and A. Dabas, *Opt. Eng.* **40**, No. 1, 115–125 (2001).
6. I.N. Smalikho, *J. Atmos. and Ocean. Technol.* **20**, No. 2, 276–291 (2003).
7. T. Gal-Chen, M. Xu, and W.L. Eberhard, *J. Geophys. Res.* **D 97**, No. 17, 18,409–18,423 (1992).
8. V.A. Banakh and I.N. Smalikho, *Atmos. Oceanic Opt.* **10**, No. 12, 957–965 (1997).
9. V.A. Banakh, I.N. Smalikho, F. Köpp, and Ch. Werner, *J. Atmos. and Ocean. Technol.* **16**, No. 8, 1044–1061 (1999).
10. R. Frehlich, S.M. Hannon, and S.W. Henderson, *Boundary-Layer Meteorol.* **86**, No. 1, 223–256 (1998).
11. R. Frehlich and Cornman L., *J. Atmos. and Ocean. Technol.* **19**, No. 3, 355–366 (2002).
12. F. Davies, C.G. Collier, G.N. Pearson, and K.E. Bozier, *J. Atmos. and Ocean. Technol.* **21**, No. 5, 753–761 (2004).
13. I.N. Smalikho, F. Köpp, and S. Rahm, *J. Atmos. and Ocean. Technol.* **22**, No. 11, 1733–1747 (2005).
14. S.M. Hannon and J.A. Thomson, *J. Mod. Opt.* **41**, No. 11, 2175–2196 (1994).
15. F. Köpp, *AIAA Journal* **32**, No. 4, 805–810 (1994).
16. G. Constant, R. Foord, P.A. Forrester, and J.M. Vaughan, *J. Mod. Opt.* **41**, No. 11, 2153–2173 (1994).
17. P.B. Brockman, C. Barker, G.J. Koch, D.P.C. Nguyen, and C.L. Britt, in: *Proc. 10th Coherent Laser Radar*

*Technology and Applications Conf.* Mount Hood, OR (1999), pp. 12–15.

18. F. Köpp, *Aerosp. Sci. and Technol.* **3**, 191–199 (1999).
19. M. Harris, J.M. Vaughan, K. Huenecke, and C. Huenecke, *Aerosp. Sci. and Technol.* **4**, No. 5, 363–370 (2000).
20. J.M. Vaughan and M. Harris, *Aerosp. Sci. and Technol.* **5**, No. 6, 409–411 (2001).
21. M. Harris, R.I. Young, F. Köpp, A. Dolfi, and J.-P. Cariou, *Aerosp. Sci. and Technol.* **6**, 325–331 (2002).
22. M. Keane, D. Buckton, M. Redfern, Ch. Bollig, C. Wedekind, F. Köpp, F. Berni, *J. Aircraft* **39**, No. 5, 850–861 (2002).
23. F. Köpp, I.N. Smalikho, S. Rahm, A. Dolfi, J.-P. Cariou, M. Harris, R.I. Young, K. Weekes, and N. Gordon, *AIAA Journal* **41**, No. 6, 1081–1088 (2003).
24. F. Köpp, S. Rahm, and I.N. Smalikho, *J. Atmos. and Ocean. Technol.* **21**, No. 2, 194–206 (2004).
25. F. Köpp, S. Rahm, I.N. Smalikho, A. Dolfi, J.-P. Cariou, M. Harris, and R.I. Young, *J. Aircraft* **42**, No. 7, 916–923 (2005).
26. S. Rahm, I.N. Smalikho, and F. Köpp, *J. Aircraft* **44**, No. 3, 799–805 (2007).
27. S. Rahm, and I.N. Smalikho, *J. Aircraft* **45**, No. 4, 1148–1155 (2008).
28. H. Lamb, *Hydrodynamics*, 6th ed. (Dover, New York, 1932), 592 pp.
29. T. Gerz, F. Holzäpfel, and D. Darracq, *Progr. in Aerosp. Sci.* **38**, No. 3, 181–208 (2002).
30. S.C. Crow, *AIAA Journal* **8**, No. 12, 2172–2179 (1970).
31. F. Holzäpfel, *J. Aircraft* **40**, No. 2, 323–331 (2003).
32. F. Holzäpfel, T. Hofbauer, D. Darracq, H. Moet, F. Garnier, and C. Ferreira Gago, *Aerosp. Sci. and Technol.* **7**, No. 4, 263–275 (2003).
33. F. Holzäpfel and R.E. Robins, *J. Aircraft* **41**, No. 1, 1–10 (2004).
34. C.M. Sonnenschein and F.A. Horrigan, *Appl. Opt.* **10**, No. 7, 1600–1604 (1971).
35. S.W. Henderson, P.J.M. Suni, C.P. Hale, S.M. Hannon, J.R. Magee, D.L. Bruns, and E.H. Yuen, *IEEE Trans. Geosci. and Remote Sens.* **31**, No. 1, 4–15 (1993).
36. F. Holzäpfel, T. Gerz, F. Köpp, E. Stumpf, M. Harris, R.I. Young, and A. Dolfi, *J. Atmos. and Ocean. Technol.* **20**, No. 8, 1183–1195 (2003).
37. A.Y. Jazwinski, *Stochastic Processes and Filtering Theory* (Academic Press, New York, 1970), 376 pp.
38. P. Salamitou, A. Dabas, and P.H. Flamant, *Appl. Opt.* **34**, No. 3, 499–506 (1995).
39. R. Frehlich, *J. Atmosph. and Ocean. Technol.* **14**, No. 2, 54–75 (1997).
40. D. Darracq, A. Corjon, F. Ducros, M. Keane, D. Buckton, and M. Redfern, *J. Aircraft* **37**, No. 6, 984–993 (2000).
41. R. Frehlich and R. Sharman, *J. Atmos. and Ocean. Technol.* **22**, No. 2, 117–129 (2005).
42. I.N. Smalikho, F. Köpp, and S. Rahm, in: “*Measurement of atmospheric turbulence by 2- $\mu$ m Doppler lidar. Report N 200*,” Institute of Atmos. Phys. DLR (Oberpfaffenhofen, 2004), pp. 1–37.
43. S.C. Crow and E.R. Bate, Jr., *J. Aircraft* **13**, No. 7, 476–482 (1976).